Matter

Article

A soft and fatigue-resistant material that mimics heart valves

Graphical abstract

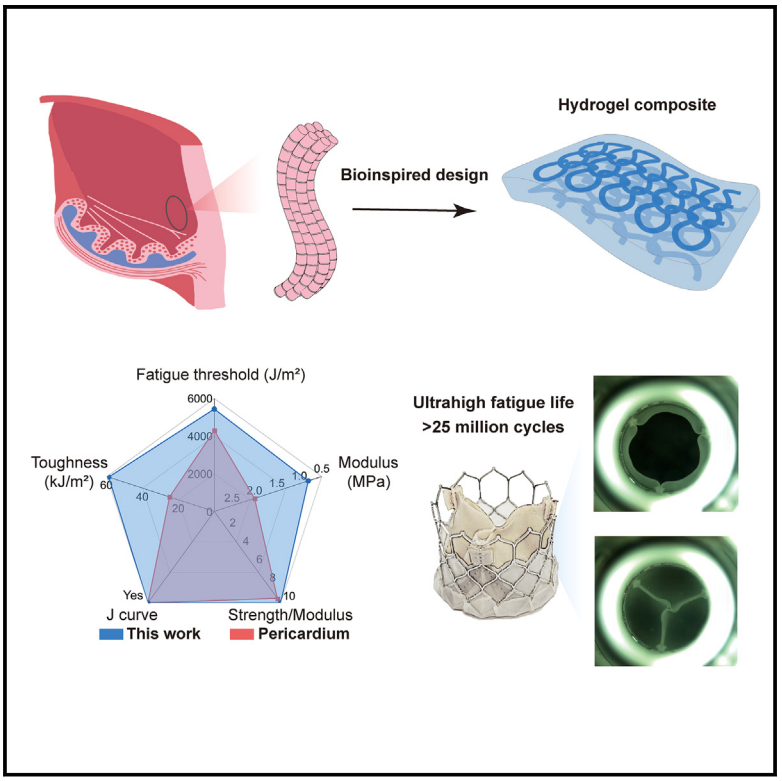

Authors

Xi Chen, Fengkai Liu, Qifeng Yu, Meng Yang, Zhigang Suo, Jingda Tang

Correspondence

tangjd@mail.xjtu.edu.cn

In brief

Inspired by the architecture of bovine pericardium, a tissue commonly used to make artificial heart valves, the authors develop a composite of a hydrogel matrix and a knitted fabric. The hydrogel composite is soft and fatigue resistant. It shows an exceptionally long fatigue life, enduring 25 million cycles of pulsatile flow, two orders of magnitude longer than the matrix. This composite may find broad applications in soft robotics and biomedicine.

Highlights

- A hydrogel composite with a fatigue life over 25 million cycles has been developed
- Improving the fatigue threshold of hydrogels by 50 times without changing its modulus
- Multi-layered crimped fiber structure inspired by the architecture of heart valves

Chen et al., 2025, Matter *8*, 101926
February 5, 2025
https://doi.org/10.1016/j.matt.2024.11.020

4 **Demonstrate**
Proof-of-concept of performance with intended application/response

CellPress

Please cite this article in press as: Chen et al., A soft and fatigue-resistant material that mimics heart valves, Matter (2024), https://doi.org/10.1016/j.matt.2024.11.020

Matter

CellPress

Article

A soft and fatigue-resistant material that mimics heart valves

Xi Chen,[1] Fengkai Liu,[1] Qifeng Yu,[3] Meng Yang,[1] Zhigang Suo,[2] and Jingda Tang[1,4,*]

[1]State Key Laboratory for Strength and Vibration of Mechanical Structures, Department of Engineering Mechanics, Xi'an Jiaotong University, Xi'an 710049, China

[2]John A. Paulson School of Engineering and Applied Sciences, Kavli Institute for Bionano Science and Technology, Harvard University, Cambridge, MA 02138, USA

[3]Shanghai NewMed Medical Corporation, Shanghai 201321, China

[4]Lead contact

*Correspondence: tangjd@mail.xjtu.edu.cn

https://doi.org/10.1016/j.matt.2024.11.020

PROGRESS AND POTENTIAL Artificial heart valves need to fulfill two fundamental mechanical requirements: a low modulus to ensure opening and closing in cyclic pulsatile flow and a high fatigue threshold to prevent crack growth. Inspired by the crimped fibrous structure of heart valves, we develop a composite of a polymer network and a knitted fabric. The fatigue threshold of the composite increases by 50 times without compromising its modulus. The composite shows an exceptionally long fatigue life, which can endure 25 million cycles of pulsatile flow even with existing flaws, two orders of magnitude longer than the matrix of polyvinyl alcohol. This work provides a critical index of performance to pursue, which is the fatigue life. The material design strategy is universal and may stimulate more hydrogel composites with ultra-high fatigue life.

SUMMARY

Bovine pericardium, a tissue commonly used to make artificial heart valves, fulfills two fundamental mechanical requirements: a low modulus to ensure opening and closing in cyclic pulsatile flow and a high fatigue threshold to prevent crack growth. The tissue consists of a soft matrix and crimped fibers. Inspired by this architecture, we develop a composite of a soft polymer matrix and a knitted fabric. When the stretch is small to modest, the knitted fabric is easily stretched, so that the composite is soft. When the stretch is large, the knitted fabric is stiff and strong, so that the composite resists fatigue crack growth. The mechanical behavior of the composite is comparable to that of bovine pericardium. The composite has an exceptionally long fatigue life, enduring 25 million cycles of pulsatile flow, two orders of magnitude longer than the polymer matrix. This soft and fatigue-resistant composite may find broad applications in biomedicine.

INTRODUCTION

Biological tissues, such as muscle, vocal cord, and heart valve, function by cyclic deformation. For instance, a heart valve regulates blood flow by opening and closing 3 billion times in the lifespan of a person.[1,2] Such a tissue fulfills two fundamental mechanical requirements: a low modulus to deform at a small force and a high fatigue threshold to resist crack growth (Figures 1A and 1B). The tissue fulfills the two requirements through a soft matrix and crimped fibers[3,4] (Figure 1C). When the stretch is small to modest, the crimped fibers de-crimp, so that the tissue has a low modulus.[5–7] When the stretch is large, particularly at a crack tip, a de-crimped fiber is stiff and deconcentrates the stress by transmitting tension over a long length of the fiber, so that the tissue has a high fatigue threshold.[8] Inspired by the fibrous structure of biological tissues, macroscopic fibers (e.g., carbon, glass fiber) have also been embedded into polymeric matrix.[9–11] The incorporation of stiff fibers can substantially increase strength and toughness.[12] However, the modulus of this composite is too high to be stretchable, which is undesirable in some applications.

Here, we develop a composite of a polymer network and a knitted fabric (Figure 1D). The polymer network functions as a soft matrix, and the knitted fabric mimics the crimped fibers. When the stretch is small to modest, the knitted fabric is stretchable, so that the composite is soft. When the stretch is large, the knitted fabric becomes stiff, so that the composite resists crack growth under cyclic stretch. The composite has mechanical properties comparable to those of bovine pericardium, a

Please cite this article in press as: Chen et al., A soft and fatigue-resistant material that mimics heart valves, Matter (2024), https://doi.org/10.1016/j.matt.2024.11.020

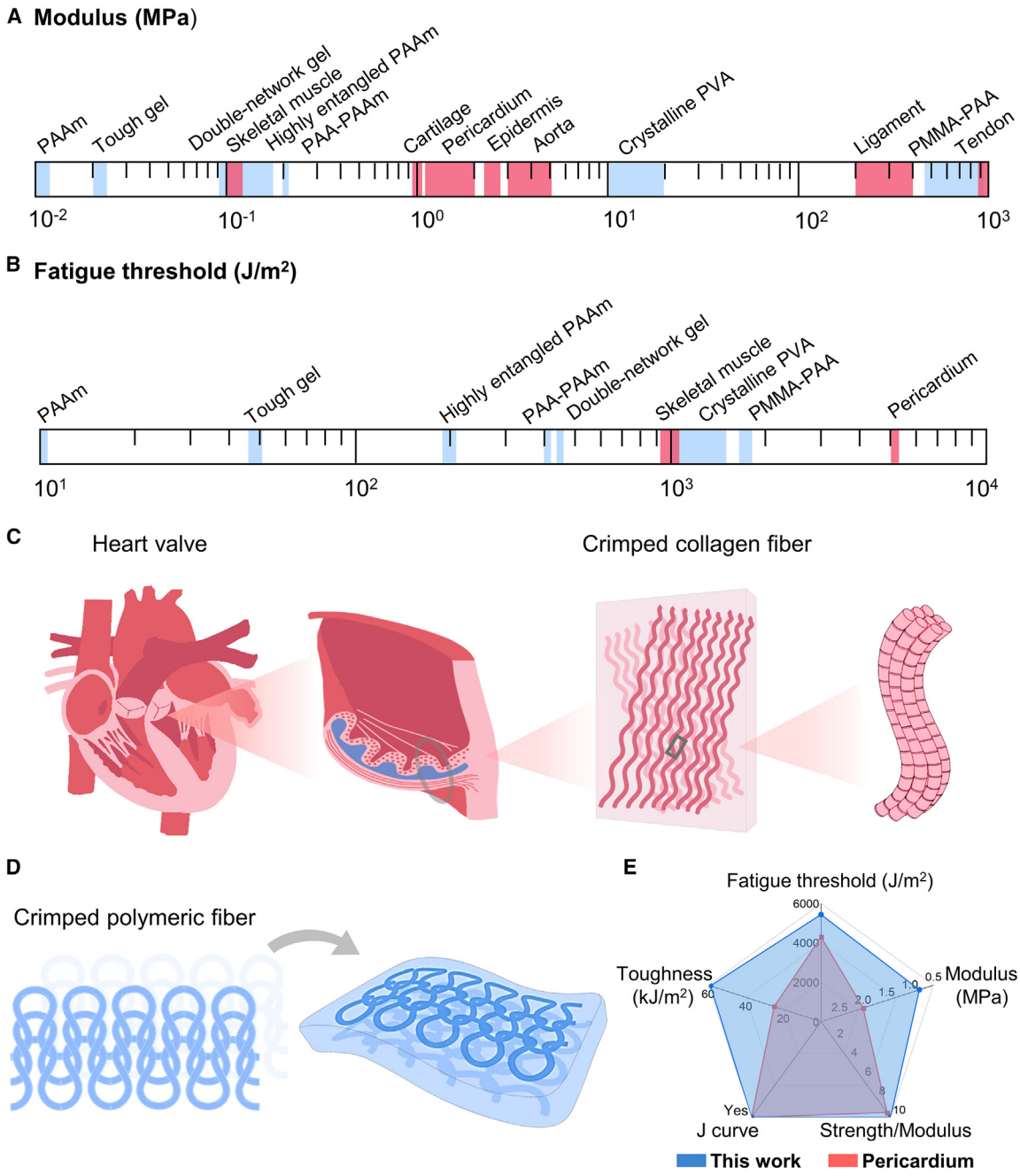

Figure 1. Modulus and fatigue threshold of soft materials

(A) Modulus of biological tissues (red) and synthetic polymers (blue).

(B) Fatigue threshold of biological tissues (red) and synthetic polymers (blue).

(C) Crimped collagen fiber in a soft extracellular matrix.

(D) Knitted fabric in a polymer matrix.

(E) Comparison of composite and bovine pericardium.

biological tissue that is used extensively in artificial heart valves. The composite has a low modulus of ~0.8 MPa and a high fatigue threshold of 5,440 J/m^2 (Figure 1E). The composite endures 25 million cycles of pulsatile flow, which is two orders of magnitude longer than the matrix.

RESULTS

Fabrication of hydrogel composites

We demonstrate this design principle using a polyvinyl alcohol (PVA) hydrogel as the soft matrix and a knitted fabric to mimic

Please cite this article in press as: Chen et al., A soft and fatigue-resistant material that mimics heart valves, Matter (2024), https://doi.org/10.1016/j.matt.2024.11.020

CellPress

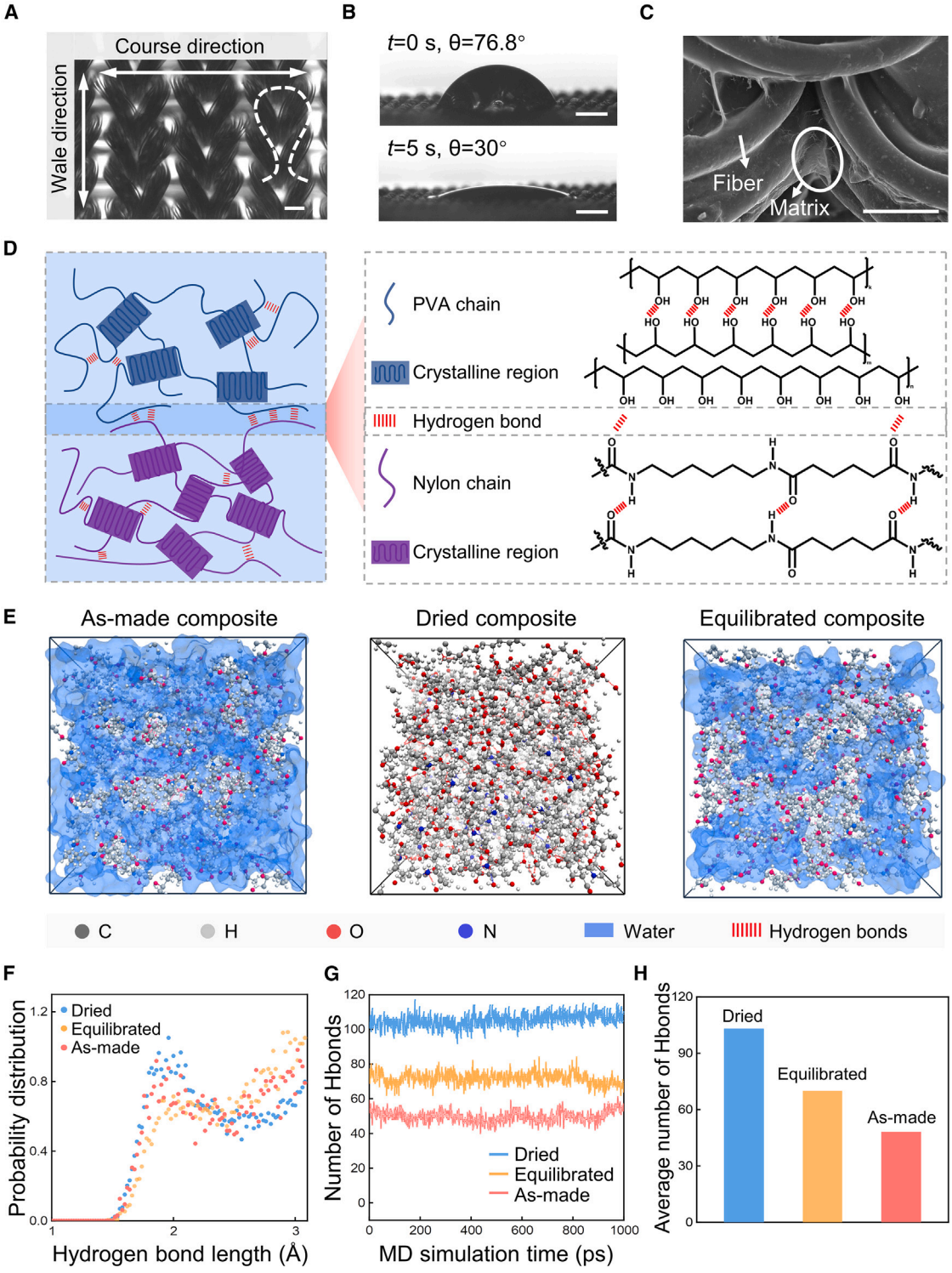

Figure 2. Structures of knitted fabric and composite

(A) Optical image of the knitted fabric. Scale bar, 100 μm.

(B) The contact angle of water on knitted fabric. Scale bar, 1 mm.

(C) Scanning electron microscopy image of the composite. Scale bar, 50 μm.

(D) Both PVA hydrogel and nylon fiber are semi-crystalline. The nylon fiber and PVA chain adhere through hydrogen bonds.

(legend continued on next page)

Please cite this article in press as: Chen et al., A soft and fatigue-resistant material that mimics heart valves, Matter (2024), https://doi.org/10.1016/j.matt.2024.11.020

crimped fibers. PVA hydrogel was selected because of its good mechanical properties and biocompatibility.[13,14] The gel is a polymer in which crystalline domains crosslink swollen polymer chains.[15–19] The knit is made of nylon fibers with periodic loops (Figure 2A). Also marked are two orientations of the knit: wale and course. Scanning electron microscopy (SEM) images show how the individual filaments are wound into fibers and how the fibers are looped into a crimped structure (Figure S1). The diameters of an individual filament and fiber are ~10 and ~100 μm, respectively. The fine filament causes minimal damage to the matrix during deformation.[20] It is also noted that a small amount of spandex fiber is typically added to enhance the formability of the fabric in industrial production. The knit shows good hydrophilicity. The contact angle of water on the knit decreases to 30° within 5 s (Figure 2B). This enables effective penetration of the hydrogel precursor into the fabric gaps through capillarity.

We fabricate the composite as follows (Figure S2A). We dissolve PVA powder in water at an elevated temperature. We submerge the knit in the PVA solution and freeze-thaw the knit solution to form PVA crystalline regions. The PVA crystalline regions crosslink the PVA chains, resulting in a polymer network for the PVA hydrogel.[21,22] The knit and the hydrogel form a composite (Figure S2B). The composite is then dried to increase the crystallinity of the PVA matrix (Figure S2C). Submerged in water, the composite swells, but the PVA with increased crystallinity reduces the amount of swelling in equilibrium.[23] The composite with fully swollen PVA hydrogel has good flexibility and stretchability (Figure S2D). SEM images show that the knit is well covered by the matrix, with matrix filling between the nylon fibers, as well as nylon fiber bundles (Figure 2C). To assess the adhesion between PVA and nylon, fiber pull-out tests are conducted to measure the interface strength[9,24] (Figure S3). The nylon fiber is gradually pulled out from the PVA matrix and breaks during the pull-out process, indicating a good adhesion. The interfacial strength is 0.35 MPa.

We attribute the strong adhesion to multiple hydrogen bonds between the nylon and PVA during the preparation process. The nylon has amide groups and carbonyl groups, and PVA has hydroxyl groups. These groups form hydrogen bonds in the crystalline regions in nylon and in PVA, as well as between nylon and PVA chains (Figure 2D). In the freeze-thaw process of the composite, crystalline regions form in the PVA, creating a three-dimensional polymer network. The hydroxyl groups on the PVA establish hydrogen bonds with the carbonyl groups on the nylon fibers.[25] The subsequent drying process reduces the binding of water molecules to hydroxyl groups on PVA, which disrupts the formation of hydrogen bonds between nylon and PVA chains. By contrast, if there is no drying treatment, these hydrogen bonds are easily disrupted by water molecules when the matrix undergoes significant swelling.

To understand the molecular picture, we conduct a molecular dynamics (MD) simulation between the nylon and PVA chains using the open-source software GROMACS. For short segments, hydrogen bonds exist between nylon and PVA, PVA and PVA, and nylon and nylon (Figure S4). We establish three model systems. For a mixture of nylon and PVA without any water, we fix a ratio of the number of repeat units of nylon over that of PVA at 1:6. For an as-made composite, we fix a ratio of the numbers of repeat units of nylon, PVA, and water molecules at 1:6:20. For a composite equilibrated with pure water, we fix a ratio of the numbers of repeat units of nylon, PVA, and water molecules at 1:6:10. For each model system, the molecular configuration is first adjusted to minimize the potential energy. Then, MD simulation is carried out to account for the kinetic energy (Figure 2E). The probability distribution of the lengths of hydrogen bonds between nylon and PVA has a peak at 1.96 Å for the dried PVA-nylon mixture, 1.96 Å for the as-made composite, and 2 Å for the composite equilibrated with pure water (Figure 2F). These short lengths of hydrogen bonds indicate the formation of strong hydrogen bonds in MD simulations.[26] For each model system, we count the number of hydrogen bonds between nylon and PVA over the simulation time (Figure 2G). The average number of hydrogen bonds per repeat unit of PVA is 0.35 for the dry PVA-nylon mixture, 0.15 for the as-made composite, and 0.24 for composite equilibrated with pure water (Figure 2H). These simulations neglect phase separation. In the hydrogel, the nylon and PVA form dry domains that function as crosslinks. This phase separation requires larger time and length scales for all-atom simulations.

To demonstrate the unique role of the PVA hydrogel, we alternatively use polyacrylamide (PAAm) hydrogel to prepare the composite. The fiber bundles can easily separate from the PAAm matrix after swelling (Figure S5), despite the surface treatment of the knit.[27] This indicates that the PAAm matrix does not have adequate interactions with nylon fibers after swelling, resulting in the weak interface bonding.

Tension behavior

We demonstrate that the composite has outstanding tension properties that are comparable to those of bovine pericardium. The composite exhibits a J-shaped stress-stretch curve (Figure 3A). When the stretch is small to modest, it has a low modulus for easy stretching. In this state, the contribution of the knit to the modulus is minimal because of the crimped structure, and the soft matrix primarily determines the modulus. When the stretch is large, the fiber straightens through bending that results in high strength. The modulus of the composite lies between that of the PVA matrix and bovine pericardium, but the strength of the composite is higher than both of them. To elucidate the role of the crimped structure, we also prepare composite reinforced by woven fabric with straight fibers.[28] This composite has a linear stress-stretch curve, lacking the J-curve behavior and large stretchability[9] (Figure S6). We compare various materials and tissues in the plane of strength

(E) Molecular dynamics simulation of the material system, including nylon, PVA, and water.
(F) The probability distributions of hydrogen bond length between PVA and nylon.
(G) The number of hydrogen bonds fluctuates with the simulation time.
(H) The average number of hydrogen bonds changes with the number of water molecules.

Please cite this article in press as: Chen et al., A soft and fatigue-resistant material that mimics heart valves, Matter (2024), https://doi.org/10.1016/j.matt.2024.11.020

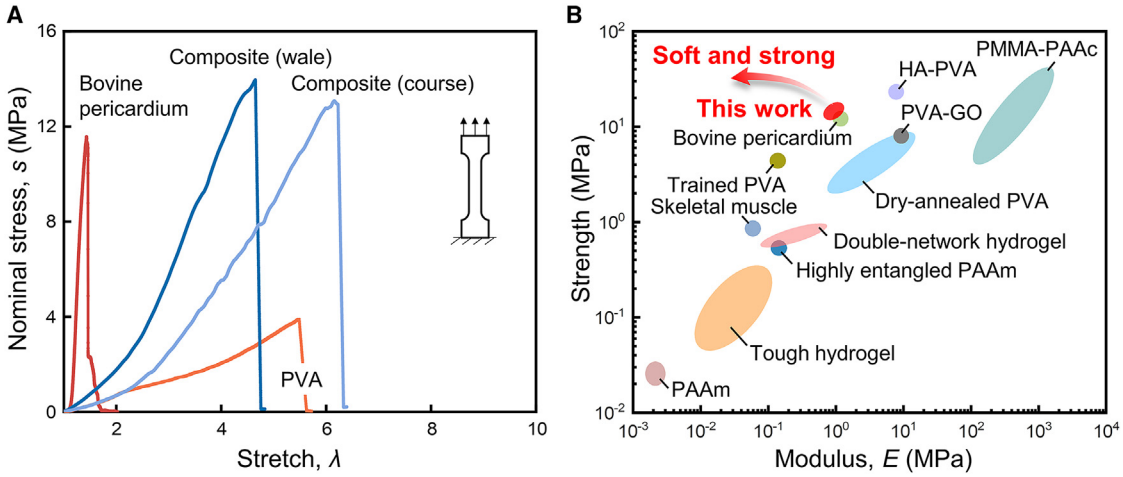

Figure 3. Tensile test of various materials

(A) Stress-stretch curves of bovine pericardium, hydrogel composite, and PVA matrix.

(B) Comparison of various materials on the plane of modulus and strength.

and modulus (Figure 3B). The composite exhibits a low modulus of 0.8–1 MPa and a high strength of 13 MPa, comparable to that of bovine pericardium.[28] The strength of the composite is close to that of the fabric, measured at 15 MPa. Because fiber breakage is a major contributor to the strength (Figure S7). Then, we also characterize the fracture properties of the composite. The critical stretch of the composite surpasses that of both the PVA matrix and bovine pericardium (Figure S8A). The crack propagates in the composite when the fiber breaks, so that the stress-stretch curve shows a zigzag shape (Figure S8B). The stress at the crack tip deconcentrates to improve the fracture toughness. We compare various materials and tissues in the plane of the toughness and modulus (Figure S8C). The composite exhibits a low modulus and a high toughness of 53 kJ/m^2, higher than muscle and bovine pericardium.

Fatigue resistance

We characterize fatigue crack growth in the course direction as follows. Introduce a precut in each specimen in the course direction, and apply the cyclic load of a fixed amplitude of energy release rate G. In our experiment, the shortest crack growth that can be resolved in a microscope is 20 μm, and the largest number of cycles is 30,000. Consequently, the lowest growth rate resolved in our experiment is 0.67×10^{-9} m/cycle. The cyclic stretch gradually pulls the fiber out on the crack plane, and a bridging zone is formed (Figure 4A). At the crack tip, the high stress is deconcentrated over several loops of the bridging fiber. For each amplitude of energy release rate, the crack growth, c, is a function of the number of cycles, N (Figure 4B). We further characterize fatigue crack growth in the wale direction. When the sample is cyclically stretched, the fiber aligns perpendicularly to the crack plane and forms a fiber-bridging zone instantly (Figure 4C). For each amplitude of energy release rate, c is also a function of N (Figure S9).

We identify two thresholds, G_a and G_b. When $G < G_a$, the crack does not grow. When $G_a < G < G_b$, the crack grows and arrests. The fiber forms a bridging zone and does not break. The bridging fiber deconcentrates stress at the crack tip and inhibits further crack growth. When $G > G_b$, the bridging fiber breaks, and the crack does not arrest (Figures S10 and S11). The crack arrest length, c_a, is a function of the amplitude of energy release rate, G (Figure 4D). For the precut in course direction, G_a = 124 J/m^2 and G_b = 4,880 J/m^2. At G_b, the crack arrest length is c_a = 3.73 mm. For the precut in wale direction, G_a = 1,450 J/m^2 and G_b = 5,173 J/m^2. At G_b, the crack arrest length is c_a = 1.28 mm. The crack growth in the two directions has similar values of G_b. This observation is not unexpected because G_b denotes the fatigue resistance of the material to fiber break, and the strength of the fiber is independent of the direction of crack growth. The crack growth in the two directions has markedly different values of G_a.

To understand the difference, we visualize the evolution of knit geometry by finite element simulations. The knit structure in simulation closely mimics that used in the experiments. The number of loops in the simulation does not completely match the experimental conditions, as doing this would significantly increase computational complexity. For the crack in course direction, the bridging fiber forms by fiber pull-out, and the crack grows (Figure 4E; Video S1). In contrast, for the crack in the wale direction, the bridging zone forms by fiber rearrangement. As stress transfers to the knit loops by contact, friction is induced. The maximum friction force of the first loop at the crack front is a function of normalized stretch (Figure 4F). For the crack growth in the course direction, the contact friction increases to 0.082 N, then drops to 0 at a normalized stretch of 1.18. The low friction is insufficient to maintain the knit geometry structure, resulting in the pull-out of the fiber. For the crack growth in the wale direction, the friction between loops increases and fluctuates around a high friction of 3 N. This friction is one order of magnitude higher than that of the crack growth in the course direction, so that the fiber is difficult to pull out. The difference in friction leads to different bridging zones, which influences G_a greatly. We further simulate a sparse knit structure with a lower

Please cite this article in press as: Chen et al., A soft and fatigue-resistant material that mimics heart valves, Matter (2024), https://doi.org/10.1016/j.matt.2024.11.020

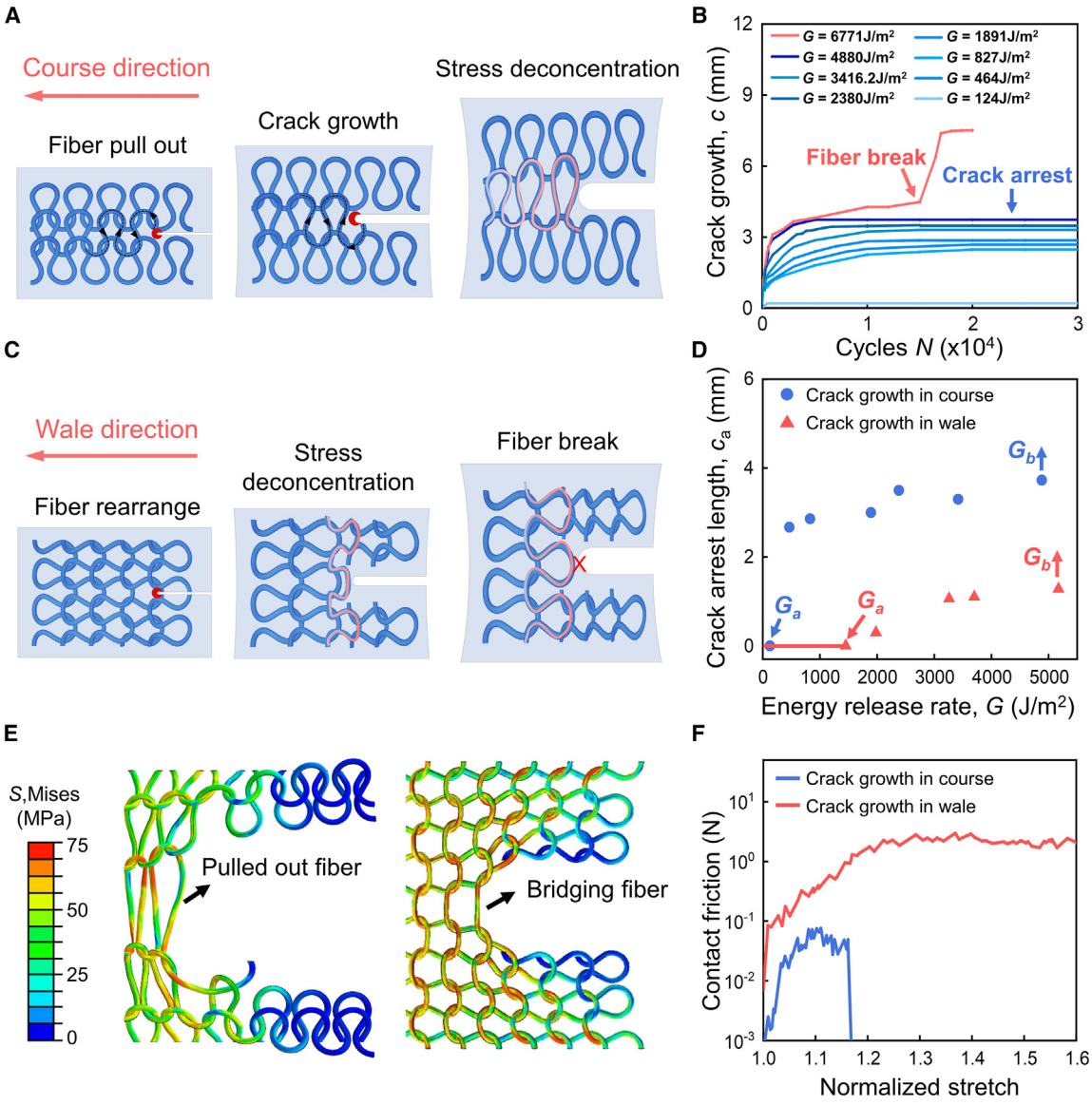

Figure 4. Fatigue crack growth

(A) Schematic of the fatigue crack growth in course direction.
(B) Crack growth c as a function of the cycle number N.
(C) Schematic of the fatigue crack growth in the wale direction.
(D) Crack arrest length c_a as a function of energy release rate G.
(E) Stress contour of the knit with a precut during stretching.
(F) The contact friction of loops is different for the crack growth in two directions.

density and sparser loop arrangement. Figure S12 shows that the crack grows to a longer distance by fiber pull-out under the same stretch. This proves the rationale to choose a fabric with dense loop structure as the fabric in our experiment. Moreover, we find that when a loosely knitted fabric is used, the precut position can influence the mechanical properties. If the crack tip is in the matrix, then the crack will propagate in the matrix first. If the crack tip is in front of the fiber, then it can propagate when the fiber breaks (Figure S13). In this work, we use a densely knitted fabric, and the precut location almost does not affect the fiber breakage location. This knit structure features high loop density and increased friction, which prevents the fibers from slipping out of the loops and minimizes the impact of precut location.[29,30] Additionally, we study the damage of the uncut composite under cyclic stretch with a prescribed amplitude (Figure S14). The stress-stretch curve can shake down to a steady curve after 30,000 cycles. The SEM image shows that the fibers do not damage the matrix.

Please cite this article in press as: Chen et al., A soft and fatigue-resistant material that mimics heart valves, Matter (2024), https://doi.org/10.1016/j.matt.2024.11.020

CellPress

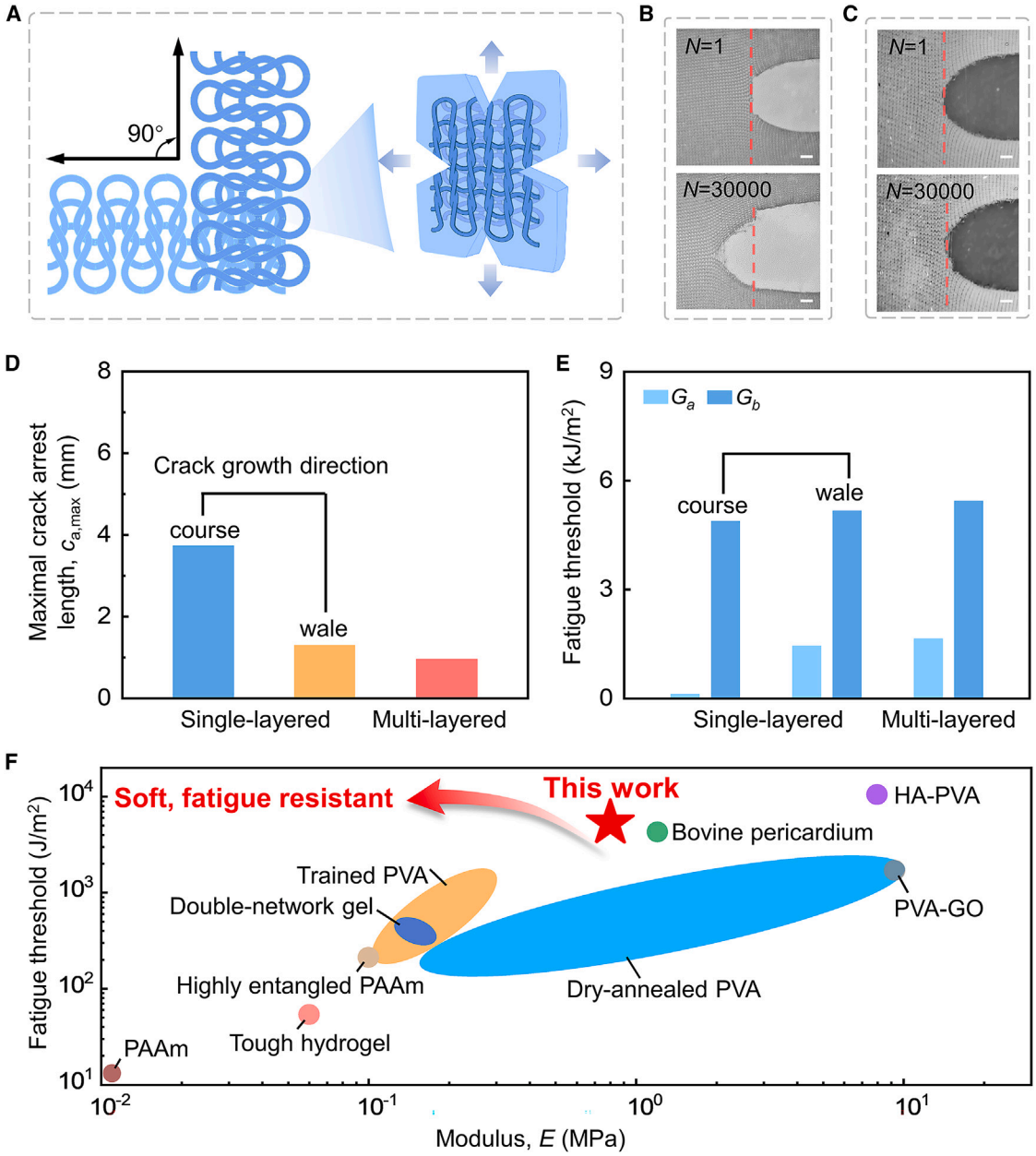

Figure 5. Fatigue of multi-layered composite

(A) Schematic of multi-layered composite.

(B and C) At the same stretch, the fatigue crack grows in the (B) single-layered composite, but it stops in the (C) multi-layered composite. Scale bar, 1 mm.

(D and E) Saturated crack arrest length (D) and fatigue threshold for single-layered and multi-layered composites (E).

(F) Comparison of modulus and fatigue threshold of various materials.

Multi-layered composite

For hydrogel-fabric composite, the knit structure is damaged to establish a fiber-bridging zone, which resists fatigue crack growth. The large crack arrest length leads to the material damage, which is undesirable for applications. How to resist fatigue crack growth in multiple directions with minimal crack arrest length remains an issue. Biological tissues can resist fatigue crack growth in all directions, since the tissues often have multiple layers of collagen fibers aligned in different directions. To visualize the crimped structure of collagen fibers, we conduct second harmonic generation (SHG) observations on bovine pericardium.[31,32] The SHG images show the multi-layered structure of crimped collagen fibers, where different layers have different predominant fiber directions (Figure S15).

Inspired by this structure, we stack two layers of knits orthogonally and embed them into a hydrogel matrix (Figure 5A). In this

Please cite this article in press as: Chen et al., A soft and fatigue-resistant material that mimics heart valves, Matter (2024), https://doi.org/10.1016/j.matt.2024.11.020

design, the vertical and horizontal directions are symmetric. Thus, one direction is selected to characterize the fatigue resistance. We compare the crack growth between single-layered and multi-layered composites. At the same stretch of $\lambda = 2$, the crack in course direction grows a length of 3 mm in the single-layered composite (Figure 5B), but the crack almost does not extend in the multi-layered composite (Figure 5C). This is because the fibers at the crack tip need to be pulled out over a longer distance to form an effective fiber bridge zone when crack growth in course direction of single-layered composite. In contrast, for multi-layered composites, fibers at the crack tip do not slip out of the loop in multiple directions. This allows a fiber-bridging zone to form without fiber pull-out, resisting crack growth. We record the relation between c and N, and plot the crack arrest length c_a as a function of the amplitude of energy release rate G (Figure S16). Then, we summarize the fatigue thresholds and maximal crack arrest length of multi-layered and single-layered composites. The maximal crack arrest length reaches 0.96 mm for the multi-layered composite, which is smaller than that of the single-layered composite in two directions (Figure 5D). The fatigue threshold G_b of the multi-layered composite is 5,440 J/m^2 (Figure 5E). G_b is comparable for three cases, since it is related to the break of fiber with the same strength (Figure S17). The threshold G_a of the multi-layered composite is 1,650 J/m^2, close to that of crack growth in the wale direction of the single-layered composite, but significantly higher than that of course direction. We compare the fatigue threshold G_b versus modulus for various hydrogels and biological tissues (Figure 5F). Bovine pericardium exhibits a high fatigue threshold of 4,300 J/m^2 and a low modulus of ~1 MPa.[8] By mimicking its multi-layered structure of crimped fiber, the composite in this work can also achieve a high fatigue threshold of 5,440 J/m^2, while maintaining a low modulus of ~0.8 MPa. The results confirm that the multi-layered structure can resist fatigue crack growth with minimal crack arrest length.

The multi-layered composite can mimic the bovine pericardium in many aspects. We compare the mechanical properties between the composite, bovine pericardium, and PVA matrix (Figure S18). The modulus of the composite is close to that of the PVA matrix and is lower than that of bovine pericardium. The strength of the composite is 13 MPa, close to that of bovine pericardium (12 MPa). Moreover, the composite exhibits a toughness of 53 kJ/m^2, markedly higher than that of the PVA matrix (2.8 kJ/m^2) and that of bovine pericardium (23 kJ/m^2). Additionally, the composite has a fatigue threshold of 5,440 J/m^2, comparable to that of bovine pericardium (4,300 J/m^2), and 50 times higher than that of the PVA matrix (121 J/m^2).

Ultrahigh cycle fatigue test

In the following, we aim to evaluate whether this hydrogel has the potential to be used in artificial heart valves with an extraordinarily long fatigue life. When a person has heart valve disease and requires replacement surgery, the minimally invasive surgery can be conducted.[33] This requires the artificial heart valve to be cut into leaflets and sutured onto metal scaffolds. The entire assembly, including the metal scaffold and leaflets, is delivered to the lesion position via a catheter. To verify whether the fatigue life of synthetic materials can meet the requirement of artificial heart valves, accelerated fatigue tests are conducted in accordance with ISO 5840 standards. The composite is cut into three leaflets, which are sutured to a metal holder (Figure 6A). In this process, suture holes are introduced into the composite as initial flaws (Figure S19), which may propagate during the fatigue test.[8,34] The assembly of leaflets and metal holder is mounted onto an accelerated wear testing machine to undergo cycles of pulsatile flow at a frequency of 15 Hz (Figures 6B and 6C). A high frequency is used to reduce the long duration of fatigue tests. For the normal physiological frequency, the same cycle number could take several years or even decades. For comparison, the leaflets made of the PVA hydrogel are also fabricated. The PVA hydrogel valve is soft enough to allow smooth opening and closing (Video S2), but it grows multiple cracks after ~200,000 cycles (Figure 6D). In contrast, the composite valve remains intact even after ~25 million cycles (Figure 6E; Video S3). The composite shows an exceptionally long fatigue life, which is two orders of magnitude higher than that of PVA hydrogel and one order of magnitude higher than that of thermoplastic polyurethane (TPU)[8] (Figure 6F).

We examine the tested composite and find that the suture hole does not grow any cracks after ultrahigh cycles of loading (Figure S20A). The surface morphology of the leaflet close to the suture hole shows negligible damage to the matrix (Figure S20B). Additionally, the cross-sectional image shows that the multi-layered fabrics remain interconnected through the matrix, without obvious delamination (Figure S20C). We also evaluate the suture retention capability of the composite. The PVA hydrogel can be easily cut by the suture thread, while the composite can resist crack propagation (Figure S21). The composite exhibits a peak suture force of 18 N, significantly higher than that of the PVA hydrogel, 0.4 N.

DISCUSSION

We have developed a knit-hydrogel composite with mechanical properties comparable to bovine pericardium. Inspired by the multi-layered structure of collagen fibers in the biological tissue, we embed multi-layers of knitted nylon fabrics in a PVA hydrogel matrix. When the stretch is small to modest, the knitted fabric is easily stretched, so that the composite is soft. When the stretch is large, the knit becomes stiff and resists crack growth under cyclic stretch, so that the composite has a high fatigue threshold. The knit amplifies the fatigue threshold by 50 times without increasing the modulus. The composite shows an exceptionally long fatigue life, which can endure 25 million cycles of pulsatile flow even with flaws, two orders of magnitude longer than that of the matrix. The fatigue life of this hydrogel composite is among the highest ever reported. This strategy for designing soft and fatigue-resistant material is universal for other polymeric composites. It is hoped that such a bioinspired composite will promote applications such as soft robotics, flexible sensors, and tissue implants.

EXPERIMENTAL PROCEDURES

Materials

PVA (molecular weight 146,000–186,000; 99+% hydrolyzed) and *N,N′*-methylene bis(acrylamide) (MBAA) were purchased from Sigma-Aldrich.

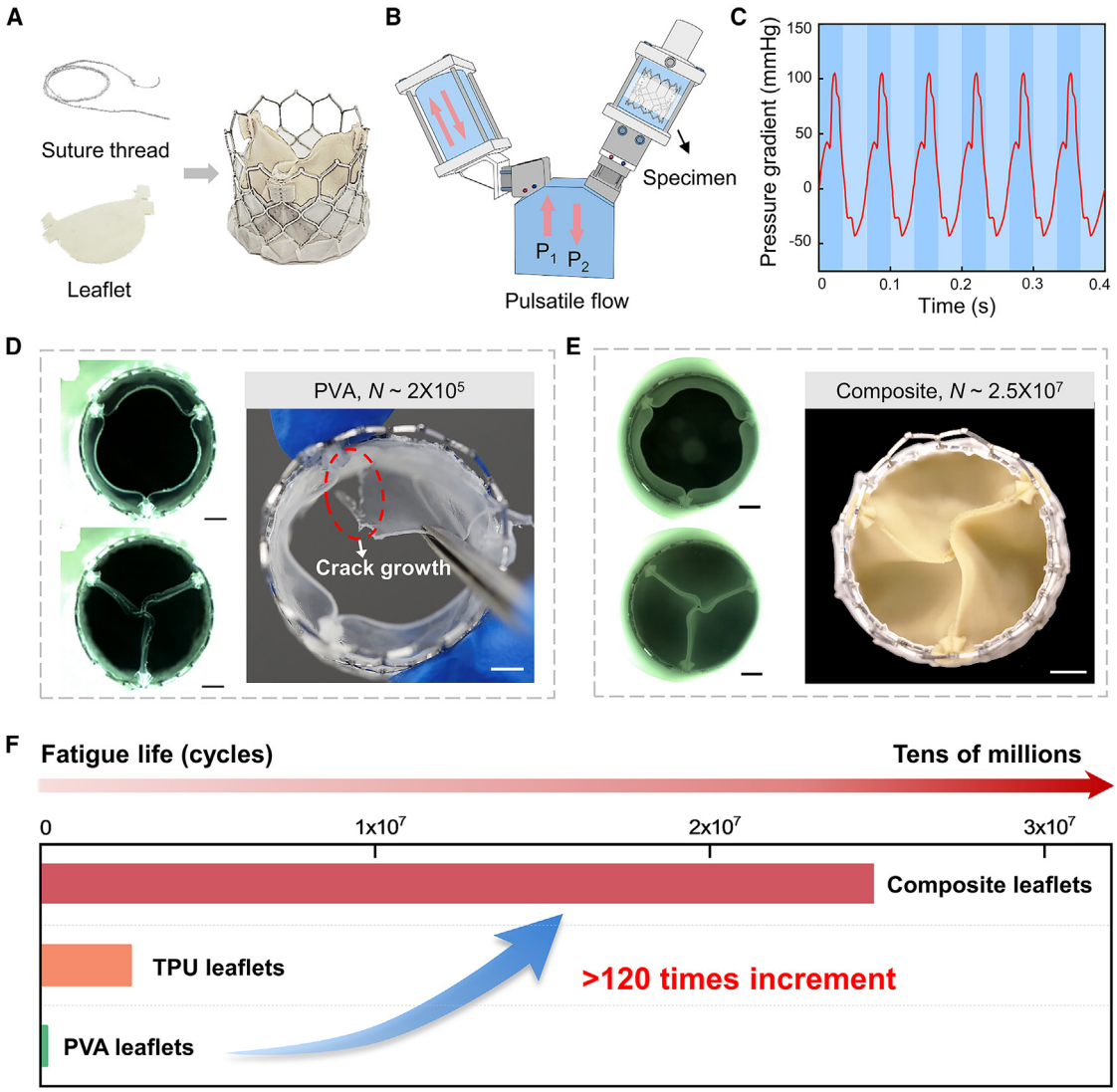

Figure 6. Ultrahigh cycle fatigue test

(A) Schematic of the leaflets stitched to a metal holder, where the suture hole may grow cracks.
(B) The specimen is mounted onto an accelerated wearing test machine, along with the metal holder.
(C) Cyclic pulsatile flow is applied to test the fatigue life.
(D) The PVA hydrogel grows multiple cracks after 200,000 cycles.
(E) The composite remains intact after 25 million cycles. Scale bar, 1 cm.
(F) Fatigue life of the leaflets made of PVA, TPU, and composite.

Acrylamide (AAm) was purchased from Macklin. 2-Hydroxy-4′-(2-hydroxyethoxy)-2-methyl-propiophe (I2959) was purchased from Aladdin. The deionized water was purified by BDPV-II-20H. All the chemicals were used as purchased without further purification. The knitted fabric, nylon fiber, and suture thread were purchased from a local market. The knitting method was weft knitting. The fabric weight was 90 g/cm^2. The underfill coefficient was 13. The wale-wise density of the fabric was 108 loops/50 mm, and the course-wise density of the fabric was 134 loops/50 mm. Commercial-grade bovine pericardium membranes treated with glutaraldehyde were provided by Shanghai NewMed Medical Company (China). The bovine pericardium for mechanical tests here was chosen by small-angle light scattering with the same collagen fiber orientation of the previous work.[8,35]

Synthesis of hydrogels

The fabric was initially soaked overnight in a mixed solution containing 90 wt % alcohol and 10 wt % acetone to eliminate the oil and wax on the fabric surface. The preparation process for the composite with a PVA hydrogel matrix was as follows. We used a glass plate and a silicone spacer as a mold, with the silicone spacer being slightly thicker than the fabric. PVA particles were added to deionized water and dissolved in an oven at 95°C to form a homogeneous solution with a PVA mass fraction of 10 wt %. We poured the PVA solution onto the glass plate, ensuring that its thickness was approximately half that of the silicone spacer. After placing the fabric in the mold, the hydrophilicity of the fabric allowed the solution to penetrate the holes between fabric yarns within a few seconds. We then added excessive PVA solution to fill the entire mold. We covered the mold with another glass plate. The mold was frozen at −20°C

Please cite this article in press as: Chen et al., A soft and fatigue-resistant material that mimics heart valves, Matter (2024), https://doi.org/10.1016/j.matt.2024.11.020

for 12 h and subsequently thawed at room temperature for 3 h. After this, we carefully removed the mold and obtained the as-made composite. The composite was then dried in an oven at 40°C for 2 h to enhance the interface. Finally, the composite was immersed in deionized water for 24 h to achieve complete swelling.

For the composite with a PAAm hydrogel matrix, the precursor solution was prepared with 24 wt % AAm, 0.02 wt % MBAA, and 0.01 wt % I2959. The precursor solution was poured into the mold and irradiated with a UV light (40 W) for 4 h for polymerization.

The preparation process for the pure PVA hydrogel was as follows: 10 wt % PVA solution was poured into a mold assembled with two glass plates and a silicone spacer. The mold was frozen at −20°C for 12 h and subsequently thawed at room temperature for 3 h to obtain the freeze-thawed PVA hydrogel. The freeze-thawed PVA was then dried in an oven at 40°C for 2 h before fully swelling. For PVA hydrogels used in suture retention tests and ultrahigh cycle fatigue tests, the freeze-thawed PVA hydrogel was further annealed in a 100°C oven for 1 h before fully swelling to increase the fatigue resistance.

Fiber pull-out test

The fiber pull-out test was conducted using a mechanical testing machine (Shimadzu AGS-X, 100 N loading cell) at a speed of 50 mm/min. The specimen was cut into a rectangle with a gauge width of 20 mm. A nylon fiber was embedded in the middle of the specimen. The edges of the specimens were fixed to the acrylic sheets. The matrix was cut at one position to make an embedded length of fiber of 60 mm. The test schematic is shown in Figure S3. The interfacial strength was calculated through dividing the peak pull-out force by the contact area between the matrix and the yarn.

Uniaxial tensile test

The uniaxial tensile tests were conducted using a mechanical testing machine (Shimadzu AGS-X, 100 N loading cell) at a speed of 50 mm/min. The specimen was cut into a dumbbell shape with a gauge width of 2 mm and gauge length of 12 mm. The stress was defined by the force divided by the initial cross-sectional area of the specimen. The stretch was defined by the displacement divided by the undeformed length of the specimen. The modulus of the material was determined by fitting the slope of the initial linear part of the stress-stretch curve.

Fracture test

The fracture tests were conducted following the procedure described by Rivlin and Thomas.[36] The specimen was cut into a rectangle with a width of 50 mm and a height of 30 mm. For the notched specimen, a 20-mm pre-crack was introduced in the middle plane. The edges of the specimens were fixed to the acrylic sheet to ensure that the gauge height H was 10 mm. The thickness of each individual specimen was measured by a micrometer screw before the test. All specimens were stretched by the testing machine (Shimadzu AGS-X, 500 N loading cell) at a speed of 50 mm/min. The critical stretch λ_c was determined based on the starting point of crack propagation. The toughness Γ was calculated by multiplying by the initial gauge height H as $\Gamma = W(\lambda_c)H$, where W denotes the area under the stress-stretch curve of the unnotched specimen.

Fatigue test

In fatigue tests, the specimen was cyclically stretched at prescribed amplitudes of stretch λ using a mechanical testing machine with a strain rate of $1\ s^{-1}$. The test was conducted in water to prevent dehydration during the prolonged loading process. The specimen was cut into a rectangle with a width of 50 mm and a gauge height H of 10 mm. The thickness of each individual specimen was measured by a micrometer screw before test. For the precut specimen, a digital microscope was used to record the crack propagation during cyclic stretch. The energy release rate was calculated by $G = W(\lambda)H$. In the case of crack arrest, the energy release rate G was calculated using the stress-stretch curve at the 30,000th cycle. In the case of long crack propagation, the energy release rate G was calculated using the last stress-stretch curve before fiber break.

Suture retention test

The suture retention test was conducted following the procedure described by Mazza et al.[37,38] The suture thread was passed through the specimen using a needle and secured with a knot. The specimen was cut into a rectangle and clamped onto an acrylic holder. Both the gauge width and height of the specimen were 10 mm. All specimens were stretched using the mechanical testing machine at a speed of 50 mm/min, and the process was recorded using a digital microscope.

SEM characterization

SEM characterization was conducted to observe the microstructure of hydrogel composite and knitted fabric. All specimens were first swollen to equilibrium and freeze-dried using a freeze-dryer to remove the moisture. The freeze-dried specimens were then cut to observe the surface morphology and cross-section and sputtered with gold for the observation in a scanning electron microscope (Hitachi SU3500).

Contact angle measurement

The contact angle measurement was performed on a drop shape analyzer (Krüss DSA100). The liquid drop was deionized water, and the drop volume for each test was 2 μL.

SHG characterization

The bovine pericardium membranes were imaged using a multiphoton microscope (Leica SP8 DIVE) equipped with a 25× water-immersion objective lens. The excitation wavelength was set at 820 nm. The collagen fiber was detected in channel 1, which was set between 397 and 420 nm. The image resolution was set at 1,024 × 1,024 pixels, with a pixel size of 420 μm/pixel. The membranes were hydrated in PBS buffer and placed between a glass slide and a glass coverslip during imaging. The specimen size was 2 × 2 cm, and three-pixel positions on the same specimen were randomly selected during observation. The specimens were scanned from the top to the bottom in the z axis direction, capturing images of each layer at a depth of 5 μm. In the final analysis, the depths of 10 and 40 μm were taken to distinguish the main direction of collagen fibers.

Ultrahigh cycle fatigue test

In the test, the specimens were cut into three leaflets and sutured onto a metal holder. Then, the specimens were mounted to the accelerated wearing test machine (TA Instruments, USA) along with the metal holder to endure cyclic pulsatile flow. The pressure gradient of the pulsatile flow in the tests had an amplitude of 100 mm/Hg and a frequency of ∼15 Hz.

MD simulation

The open-source software GROMACS was employed to conduct MD simulation.[39] Simplified models of the molecular chains were constructed, where PVA with 15 repeating units and nylon chain with 5 repeating units were used to reduce the calculation time. Packmol, a free software package, was used to build a simulation system with periodic boundary conditions.[40] For the as-made composite, the simplified system had 20 PVA chains, 10 nylon chains, and 1,000 water molecules. For the dried composite, the simplified system included only 20 PVA chains and 10 nylon chains. For the equilibrated composite, the simplified system comprised 20 PVA chains, 10 nylon chains, and 500 water molecules. The force field was OPLS-AA for PVA and nylon and TIP3P for water. The steep descent method was used to minimize the potential energy. The three systems were subjected to 100-ps NVT (number of particles [N], volume [V], and temperature [T]) ensemble simulation, 100-ps NPT (number of particles [N], pressure [P], and temperature [T]) ensemble simulation, and 2-ns equilibrium MD simulation. During simulation, the V-rescale method was used for temperature coupling. The Parrinello-Rahman method was used for pressure coupling. The short-range van der Waals cutoff and electrostatic cutoff were set at 1.0 nm. The trajectories of the final 1,000-ps MD simulation were used for hydrogen bonds analysis. The number and length distribution of hydrogen bonds between nylon and PVA chains in the material system were statistically analyzed by GROMACS, and the trajectories were visualized using VMD software.[41]

Finite element calculation

The commercial finite element software suite ABAQUS was used to simulate the deformation of knits with precuts. The mesh element type of knit was C3D8R (Figure S22). The tangential contact friction formulation was penalty and the friction coefficient was 0.1. The normal contact was set as hard contact to avoid mesh penetration. ABAQUS/Explicit was used to avoid convergence problems due to the complex contact conditions and nonlinear effects of knit loops. The normalized stretch was defined by the displacement divided by the length when the loop came into contact. The contact friction force was defined as the maximal tangential force of the elements at the crack front.

RESOURCE AVAILABILITY

Lead contact

Further information and requests for resources and reagents should be directed to and will be fulfilled by the lead contact, Jingda Tang (tangjd@mail.xjtu.edu.cn).

Materials availability

The materials generated in this study are available from the corresponding author upon request.

Data and code availability

The data used to support the findings of this study are available from the corresponding author upon request.

ACKNOWLEDGMENTS

This research was supported by the National Natural Science Foundation of China (grant nos. 12422204 and 12172272). J.T. acknowledges the support of the K.C. Wong Education Foundation. We acknowledge the Instrumental Analysis Center of Xi'an Jiaotong University for facility support.

AUTHOR CONTRIBUTIONS

Z.S., J.T., and X.C. designed the research. X.C., F.L., Q.Y., J.T., and M.Y. performed the research. Z.S., J.T., and X.C. wrote the paper.

DECLARATION OF INTERESTS

A patent for this fabrication strategy has been filed.

SUPPLEMENTAL INFORMATION

Supplemental information can be found online at https://doi.org/10.1016/j.matt.2024.11.020.

Received: July 18, 2024
Revised: October 7, 2024
Accepted: November 14, 2024
Published: December 13, 2024

REFERENCES

1. Hinton, R.B., and Yutzey, K.E. (2011). Heart Valve Structure and Function in Development and Disease. Annu. Rev. Physiol. *73*, 29–46. https://doi.org/10.1146/annurev-physiol-012110-142145.
2. Yang, H., Ji, M., Yang, M., Shi, M., Pan, Y., Zhou, Y., Qi, H.J., Suo, Z., and Tang, J. (2021). Fabricating hydrogels to mimic biological tissues of complex shapes and high fatigue resistance. Matter *4*, 1935–1946. https://doi.org/10.1016/j.matt.2021.03.011.
3. Sharabi, M. (2022). Structural Mechanisms in Soft Fibrous Tissues: A Review. Front. Mater. *8*, 793647. https://doi.org/10.3389/fmats.2021.793647.
4. Wegst, U.G.K., Bai, H., Saiz, E., Tomsia, A.P., and Ritchie, R.O. (2015). Bioinspired structural materials. Nat. Mater. *14*, 23–36. https://doi.org/10.1038/nmat4089.
5. Dutov, P., Antipova, O., Varma, S., Orgel, J.P.R.O., and Schieber, J.D. (2016). Measurement of Elastic Modulus of Collagen Type I Single Fiber. PLoS One *11*, e0145711. https://doi.org/10.1371/journal.pone.0145711.
6. Fratzl, P., and Weinkamer, R. (2007). Nature's hierarchical materials. Prog. Mater. Sci. *52*, 1263–1334. https://doi.org/10.1016/j.pmatsci.2007.06.001.
7. Buehler, M.J. (2006). Nature designs tough collagen: Explaining the nanostructure of collagen fibrils. Proc. Natl. Acad. Sci. USA *103*, 12285–12290. https://doi.org/10.1073/pnas.0603216103.
8. Zeng, L., Liu, F., Yu, Q., Jin, C., Yang, J., Suo, Z., and Tang, J. (2023). Flaw-insensitive fatigue resistance of chemically fixed collagenous soft tissues. Sci. Adv. *9*, eade7375. https://doi.org/10.1126/sciadv.ade7375.
9. Cui, W., King, D.R., Huang, Y., Chen, L., Sun, T.L., Guo, Y., Saruwatari, Y., Hui, C.Y., Kurokawa, T., and Gong, J.P. (2020). Fiber-Reinforced Viscoelastomers Show Extraordinary Crack Resistance That Exceeds Metals. Adv. Mater. *32*, 1907180. https://doi.org/10.1002/adma.201907180.
10. Illeperuma, W.R., Sun, J.-Y., Suo, Z., and Vlassak, J.J. (2014). Fiber-reinforced tough hydrogels. Extreme Mech. Lett. *1*, 90–96. https://doi.org/10.1016/j.eml.2014.11.001.
11. King, D.R. (2022). Macroscale double networks: highly dissipative soft composites. Polym. J. *54*, 943–955. https://doi.org/10.1038/s41428-022-00646-8.
12. Li, X., and Gong, J.P. (2024). Design principles for strong and tough hydrogels. Nat. Rev. Mater. *9*, 380–398. https://doi.org/10.1038/s41578-024-00672-3.
13. Liu, X., Rao, S., Chen, W., Felix, K., Ni, J., Sahasrabudhe, A., Lin, S., Wang, Q., Liu, Y., He, Z., et al. (2023). Fatigue-resistant hydrogel optical fibers enable peripheral nerve optogenetics during locomotion. Nat. Methods *20*, 1802–1809. https://doi.org/10.1038/s41592-023-02020-9.
14. Peppas, N.A., and Mongia, N.K. (1997). Ultrapure poly(vinyl alcohol) hydrogels with mucoadhesive drug delivery characteristics. Eur. J. Pharm. Biopharm. *43*, 51–58. https://doi.org/10.1016/S0939-6411(96)00010-0.
15. Liang, X., Chen, G., Lin, S., Zhang, J., Wang, L., Zhang, P., Lan, Y., and Liu, J. (2022). Bioinspired 2D Isotropically Fatigue-Resistant Hydrogels. Adv. Mater. *34*, 2107106. https://doi.org/10.1002/adma.202107106.
16. Hua, M., Wu, S., Ma, Y., Zhao, Y., Chen, Z., Frenkel, I., Strzalka, J., Zhou, H., Zhu, X., and He, X. (2021). Strong tough hydrogels via the synergy of freeze-casting and salting out. Nature *590*, 594–599. https://doi.org/10.1038/s41586-021-03212-z.
17. Wu, S., Hua, M., Alsaid, Y., Du, Y., Ma, Y., Zhao, Y., Lo, C.-Y., Wang, C., Wu, D., Yao, B., et al. (2021). Poly(vinyl alcohol) Hydrogels with Broad-Range Tunable Mechanical Properties via the Hofmeister Effect. Adv. Mater. *33*, 2007829. https://doi.org/10.1002/adma.202007829.
18. Lin, S., Liu, J., Liu, X., and Zhao, X. (2019). Muscle-like fatigue-resistant hydrogels by mechanical training. Proc. Natl. Acad. Sci. USA *116*, 10244–10249. https://doi.org/10.1073/pnas.1903019116.
19. Lin, S., Liu, X., Liu, J., Yuk, H., Loh, H.-C., Parada, G.A., Settens, C., Song, J., Masic, A., McKinley, G.H., and Zhao, X. (2019). Anti-fatigue-fracture hydrogels. Sci. Adv. *5*, eaau8528. https://doi.org/10.1126/sciadv.aau8528.
20. Liu, D., Sun, S., Dong, G., Long, F., and Wang, M. (2023). Fatigue-resistant, single-phase stretchable materials via crack bridging. Composites, Part B *259*, 110728. https://doi.org/10.1016/j.compositesb.2023.110728.
21. Hassan, C.M., and Peppas, N.A. (2000). Structure and Applications of Poly(vinyl alcohol) Hydrogels Produced by Conventional Crosslinking or by Freezing/Thawing Methods. In Biopolymers · PVA Hydrogels, Anionic Polymerisation Nanocomposites (Springer Berlin Heidelberg), pp. 37–65. https://doi.org/10.1007/3-540-46414-X_2.
22. Hassan, C.M., and Peppas, N.A. (2000). Structure and Morphology of Freeze/Thawed PVA Hydrogels. Macromolecules *33*, 2472–2479. https://doi.org/10.1021/ma9907587.
23. Cha, W.-I., Hyon, S.-H., Oka, M., and Ikada, Y. (1996). Mechanical and wear properties of poly(vinyl alcohol) hydrogels. Macromol. Symp. *109*, 115–126. https://doi.org/10.1002/masy.19961090111.

24. King, D.R., Sun, T.L., Huang, Y., Kurokawa, T., Nonoyama, T., Crosby, A.J., and Gong, J.P. (2015). Extremely tough composites from fabric reinforced polyampholyte hydrogels. Mater. Horiz. *2*, 584–591. https://doi.org/10.1039/C5MH00127G.

25. Cui, L., Yeh, J.-T., Wang, K., and Fu, Q. (2008). Miscibility and isothermal crystallization behavior of polyamide 6/poly(vinyl alcohol) blend. J. Polym. Sci. B Polym. Phys. *46*, 1360–1368. https://doi.org/10.1002/polb.21470.

26. Karingithi, R.N., Shaw, C.L., Roberts, E.W., and Molina, P.A. (2008). The probability distribution function as a descriptor of hydrogen bond strength. J. Mol. Struct. THEOCHEM *851*, 92–99. https://doi.org/10.1016/j.theochem.2007.11.003.

27. Liu, Q., Nian, G., Yang, C., Qu, S., and Suo, Z. (2018). Bonding dissimilar polymer networks in various manufacturing processes. Nat. Commun. *9*, 846–911. https://doi.org/10.1038/s41467-018-03269-x.

28. Yu, H., Lin, J., Zeng, L., and Tang, J. (2024). Fatigue and fracture of soft collagenous tissues mineralized in vitro. Giant *17*, 100232. https://doi.org/10.1016/j.giant.2023.100232.

29. El-Tarfawy, S.Y. (2017). Study the relation between the yarn pulling force and the bursting strength of single jersey knitted fabric. IOP Conf. Ser. Mater. Sci. Eng. *254*, 142007. https://doi.org/10.1088/1757-899X/254/14/142007.

30. Karimian, M., Hasani, H., and Ajeli, S. (2013). Analyzing the Effect of Fiber, Yarn and Fabric Variables on Bagging Behavior of Single Jersey Weft Knitted Fabrics. J. Eng. Fiber. Fabr. *8*, 155892501300800301. https://doi.org/10.1177/155892501300800301.

31. Campion, G., Hershberger, K., Whelan, A., Conroy, J., Lally, C., and Murphy, B.P. (2021). A Biomechanical and Microstructural Analysis of Bovine and Porcine Pericardium for Use in Bioprosthetic Heart Valves. Struct. Heart *5*, 486–496. https://doi.org/10.1080/24748706.2021.1938317.

32. Wang, C., Meng, J., Qian, S., Zhou, L., Jiang, S., Jiang, R., Zhan, H., Fang, X., Liu, Y., Ding, Z., and Liu, Z. (2023). Quantification methodologies on organization and morphology features of fiber-like structures: A review. J. Innov. Opt. Health Sci. *16*, 2230012. https://doi.org/10.1142/s1793545822300129.

33. Arsalan, M., and Walther, T. (2016). Durability of prostheses for transcatheter aortic valve implantation. Nat. Rev. Cardiol. *13*, 360–367. https://doi.org/10.1038/nrcardio.2016.43.

34. Chen, X., Lin, J., Yang, H., and Tang, J. (2024). Flaw sensitivity of hydrogels with dynamic covalent bonds. Extreme Mech. Lett. *67*, 102129. https://doi.org/10.1016/j.eml.2024.102129.

35. Tang, J., Lin, J., and Wang, T. (2024). Cracking of Soft Collagenous Tissues under Suture Retention. J. Mech. Phys. Solid. *188*, 105682. https://doi.org/10.1016/j.jmps.2024.105682.

36. Rivlin, R.S., and Thomas, A.G. (1953). Rupture of rubber. I. Characteristic energy for tearing. J. Polym. Sci. *10*, 291–318. https://doi.org/10.1002/pol.1953.120100303.

37. Pensalfini, M., Meneghello, S., Lintas, V., Bircher, K., Ehret, A.E., and Mazza, E. (2018). The suture retention test, revisited and revised. J. Mech. Behav. Biomed. Mater. *77*, 711–717. https://doi.org/10.1016/j.jmbbm.2017.08.021.

38. Bircher, K., Zündel, M., Pensalfini, M., Ehret, A.E., and Mazza, E. (2019). Tear resistance of soft collagenous tissues. Nat. Commun. *10*, 792. https://doi.org/10.1038/s41467-019-08723-y.

39. Abraham, M.J., Murtola, T., Schulz, R., Páll, S., Smith, J.C., Hess, B., and Lindahl, E. (2015). GROMACS: High performance molecular simulations through multi-level parallelism from laptops to supercomputers. SoftwareX *1–2*, 19–25. https://doi.org/10.1016/j.softx.2015.06.001.

40. Martínez, L., Andrade, R., Birgin, E.G., and Martínez, J.M. (2009). PACKMOL: A package for building initial configurations for molecular dynamics simulations. J. Comput. Chem. *30*, 2157–2164. https://doi.org/10.1002/jcc.21224.

41. Humphrey, W., Dalke, A., and Schulten, K. (1996). VMD: Visual molecular dynamics. J. Mol. Graph. *14*, 33-8–27-8. https://doi.org/10.1016/0263-7855(96)00018-5.